

Insights into the Charge Storage Mechanism of Binder-Free Electrochemical Capacitors in Ionic Liquid Electrolytes

Bhupender Pal,* Abhilash Karuthedath Parameswaran, Bing Wu, Lukáš Děkanovský, Vlastimil Mazánek, Kalyan Jyoti Sarkar, Rajan Jose, and Zdeněk Sofer*



Cite This: *Ind. Eng. Chem. Res.* 2023, 62, 4388–4398



Read Online

ACCESS |



Metrics & More

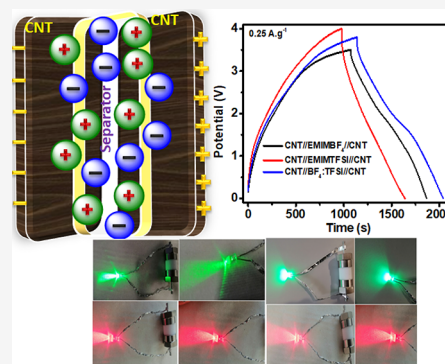


Article Recommendations



Supporting Information

ABSTRACT: Electrochemical capacitors (synonymously supercapacitors) working under an electrochemical double-layer charge storage mechanism (EDLC) are widely investigated because of their excellent power density and cycle life; however, their energy density is lower than those of lithium-ion batteries. Ionic liquids (ILs) are of great interest as electrolytes for EDLCs due to their wide operational voltage window. Here, we provide a systematic investigation on the influence of anions of ILs on the charge storage mechanism and electrochemical stability of EDLC electrodes. Two IL electrolytes, viz., [1-ethyl-3-methylimidazolium tetrafluoroborate (EMIMBF₄) and 1-ethyl-3-methylimidazolium bis(trifluoromethylsulfonyl)imide (EMIMTFSI)], having similar cations but different anions and carbon nanotube (CNT) electrodes are chosen for this study. The CNT//BF₄:TFSI//CNT-based device showed superior electrochemical performance (~69 F·g⁻¹ gravimetric specific capacitance, ~949 W·kg⁻¹ power density, and ~139 Wh·kg⁻¹ energy density at 0.5 A·g⁻¹) to CNT//EMIMBF₄//CNT and CNT//EMIMTFSI//CNT devices. The device using a mixture of BF₄:TFSI (1:0.5) electrolytes has an operating voltage of 0–3.8 V and specific capacitance retention of ~45% at 0.5 A·g⁻¹ after 500 cycles. In the case of the IL mixture (BF₄:TFSI), the combined anion structure and their properties play very crucial part in the improvement of the electrochemical performance of the CNT//BF₄:TFSI//CNT device. The assembled Teflon Swagelok-type cell could light up green (3.3 V) and red (2.1 V) light-emitting diodes for more than 5 min.



INTRODUCTION

Electrochemical capacitors (ECs) are energy storage devices with exceptional power density suitable for variety of applications such as portable/wearable electronics, medical electronics, communication sectors, electric vehicles, householding devices, and military defense systems.^{1–3} ECs refer to electrochemical double-layer capacitors (EDLCs), redox capacitors, and hybrid conductive polymer capacitors. In EDLCs, charge adsorption is accomplished upon charging the device and energy is stored in the form of a double layer at the electrode and electrolyte interface.⁴ EDLCs have excellent stability, fast charging/discharging rates, and greater power density due to the interface reversible physical adsorption rather than a redox reaction.^{5,6} The electrode materials used in EDLCs are porous carbon, graphene, reduced graphene oxide, and carbon nanotubes. Carbon nanotubes (CNTs) are getting more attention for EDLCs because of their exceptional mechanical and electrical properties and good electrolyte accessibility. Despite all these benefits, EDLCs still do not have much recognition due to their low energy density (ED) as compared to those of batteries. Therefore, considerable research is in progress to increase the energy density of these devices. The energy density of electrochemical capacitors can be increased using two parameters, specific capacitance (C_s) and operating voltage

(V), as suggested by the following equation: $E = CV^2/2$.⁷ The C_s values of electrochemical capacitors are determined mainly by electrode materials; however, the operating voltage window (V) mainly depends upon the electrochemical stability of the electrolytes.^{8,9}

Generally, in EDLC devices, organic, aqueous, ionic liquid, and polymeric electrolytes have been used.^{10–13} Due to the electrodecomposition of solvents,¹⁴ aqueous, organic, and polymeric electrolytes have limited operation voltage windows (1–3.7 V) as compared to ionic liquids (>4–5 V). Ionic liquid (IL) electrolytes are composed of inorganic anions and organic cations, which are thermally stable, nonflammable, and non-volatile compared to organic electrolytes.^{15,16} The ED of porous carbon-based electrochemical capacitors reaches 59.0 Wh·kg⁻¹ with an ionic liquid electrolyte (1-ethyl-3-methylimidazolium tetrafluoroborate) due to a higher operational voltage window (3.5 V). Some research groups have reported that mesoporous

Received: October 10, 2022

Revised: February 17, 2023

Accepted: February 19, 2023

Published: March 3, 2023



Table 1. Electrochemical Performance of Some IL-Based Electrochemical Capacitors

electrolytes	electrodes	C_s (F·g ⁻¹)	ED (Wh·kg ⁻¹)	PD (W·kg ⁻¹)	cell voltage (V)	ref
EMIMBF ₄	MnO ₂ @S/N-mesoporous carbon	200, 2 mV·s ⁻¹	85.1		3.5	25
EMIMBF ₄	O/N-doped rod-like microporous carbons	179, 0.2 A·g ⁻¹	89.5	380	3.8	26
EMIMBF ₄	TiC nanowires	169, 2 A·g ⁻¹	16.4	202	3	27
EMIMBF ₄	Ni ₃ (2,3,6,7,10,11-hexaiminotriphenylene) ₂	11	57	460	4	28
EMIMBF ₄	porous carbons (highly redox-active)	302	90.6		3.6	29
EMIMBF ₄ /PVDF	graphene nanocomposite	180, 1 A·g ⁻¹	75	200	3.5	30
EMIMBF ₄	reduced graphene oxide-IL-multiwalled carbon nanotubes	202	131.8	892.6	4.0	31
EMIMBF ₄	O/N-codoped hollow carbon nanorods	214	116.5	472	4.0	32
TMABF ₄ /EMIMBF ₄	B/N/O-doped porous carbon	209	116	400	4.0	33
EMIMTFSI	mesoporous graphene	244, 5 A·g ⁻¹	135.6	100	4	34
EMIMTFSI	IL/reduced graphene oxide	218, 1 A·g ⁻¹	45	571.4	3.0	35
EMIMTFSI/PVDF	activated carbon/Mnox@TiN nanowires@carbon nanotubes	776 F cm ⁻³ , 0.5 A cm ⁻³	61.2	200	3.5	36
EMIMFSI	micropore-rich activated carbon	93, 0.5 A·g ⁻¹	42	132	3.5	37
P444FuA	multiwalled carbon nanotubes	182, 1 A·g ⁻¹	138.1	420	4.6	38
BMIMPF ₆	carbon nanosponge	290	204		4	39
EMIMBF ₄	multiwalled carbon nanotubes	55, 0.5 A·g ⁻¹	94	874	3.5	this work
EMIMTFSI	multiwalled carbon nanotubes	33, 0.5 A·g ⁻¹	74	999	4.0	this work
EMIMBF ₄ :EMIMTFSI	multiwalled carbon nanotubes	69, 0.5 A·g ⁻¹	139	949	3.8	this work

activated carbon with an EMIMBF₄ electrolyte has a higher operational voltage window up to 3.8 to 4 V, significantly improving the ED of the device. The C_s and operational voltage window of the electrochemical capacitors are affected by the chemical structure of electrolytes and ion distribution adjacent to the charged electrode. Molecular dynamic simulations have shown that at various potentials, changing the cation could considerably change the dynamics and structure of the EDLC. An enhanced electrochemical stability has been reported for *N*-alkyl-*N*-(methyl-imidazolium) bis(trifluoro-methyl-sulfonyl-imide) and *N*-alkyl-*N*-(methyl-pyrrolidinium) bis(trifluoro-methyl-sulfonyl)-imide just by extending the alkyl substitute chain length;^{17,18} however, a decrease in potential window was also reported for *N*-alkyl-*N*-methyl-pyrrolidinium bis(trifluoro-methyl-sulfonyl)-imide by changing the chain length of alkyl substitutes.¹⁹ Sedev et al.²⁰ also reported that the double-layer capacitance decreases when increasing the 1-alkyl-3-ethyl-imidazolium chloride alkyl chain length with carbon electrodes. Likewise, 1-butyl-3-methyl-imidazolium tetrafluoro-borate has shown less double-layer C_s than 1-ethyl-3-methyl-imidazolium tetrafluoro-borate²¹ and tetra-alkylammonium tetrafluoroborate (like ethyl, propyl, butyl, and hexyl) has displayed size-dependent double-layer capacitance.²² Despite these benefits, there is not much systematic and comprehensive study about variation in the anion structure of ILs and their effect on electrochemical properties of EDLC devices; however, there are few reports about the effect of the cation structure of ILs on EDLC devices.^{19,23,24} The electrochemical performances of some IL-based electrochemical capacitors are demonstrated in Table 1.

In addition, the double-layer capacitance values of ionic liquids are also affected by electrode materials.^{40–42} A direct comparison between those reported in the literature is not feasible due to the wide range of electrode materials. Based on similar electrode constituents, it is essential to study the effect of only anions/cations of ionic liquids on the ED of EDLCs. Therefore, the focus of the current study is to relate the properties of EDLCs fabricated with the same electrode material with electrolytes of different types of ionic liquids (same cations

but different anions). This study uses CNTs as a model electrode material due to their high porosity, uniformity, and superior electric conductivity. The as-prepared symmetric electrochemical capacitors (CNT//EMIMBF₄//CNT, CNT//EMIMTFSI//CNT, and CNT/BF₄TFSI//CNT) exhibit excellent electrochemical performance and cycle life even at higher current densities. Additionally, the devices can considerably light up green (3.3 V) and red (2.1 V) light-emitting diodes (LEDs) for more than 5 min.

EXPERIMENTAL DETAILS

Materials. CNTs were purchased from OCSiAl, Germany; 1-ethyl-3-methylimidazolium tetrafluoroborate (EMIMBF₄) and 1-ethyl-3-methylimidazolium bis(trifluoromethylsulfonyl) imide (EMIMTFSI) ionic liquid electrolytes were used as received (neat ionic liquid). The chemicals and reagents were of analytical grade and used without further purification.

Pre-treatment and Dispersion of Carbon Nanotubes (CNTs). Previously reported procedures were used to prepare CNTs.⁴³ Typically, 3 g of CNTs was dispersed into H₂SO₄ (96 wt %, 600 mL) by vigorous stirring; after 30 min, 0.5 g of KMnO₄ was added, and then the solution was stirred for 3 h at room temperature and was consequently purged in 5 L of deionized water. The oxidized CNTs were decanted three times, separated by vacuum filtration, and then washed with deionized water and ethanol four to five times. Finally, the sample was dried at room temperature in a vacuum oven for 50 h.

Preparation of the CNT Film as an Electrode Material. A total of 150 mg of as-pretreated CNTs was dispersed in 500 mL of deionized water using an Ultraturax T18 dispersing unit for 4 h to get stable dispersion. Finally, the dispersion was carefully filtered through a porous cellulose membrane (pore size: 0.22 μm) with the aid of vacuum filtration. The resultant CNT film was washed several times with deionized water. Subsequently, the CNT film was allowed to dry at room temperature for 3 to 4 days to ensure proper settlement of the film. Then, the CNT film was dipped in acetone solution for 5 h to remove the cellulose membrane (filter paper); finally, a

freestanding flexible CNT film was obtained after drying for 12 h.

Electrolyte Preparation. In this study, three types of ionic liquid electrolytes were used, viz., EMIMBF₄, EMIMTFSI, and their mixture (1:0.5). A mixture of EMIMBF₄:EMIMTFSI ionic liquid electrolytes was prepared in a ratio of 1:0.5 and further used for full device fabrication. The EMIMBF₄ and EMIMTFSI ionic liquid electrolytes were used individually as received (neat) for full device fabrication.

Characterizations. The phase identification and crystal structures of CNTs were investigated by X-ray diffractometry. The size and shape of the as-prepared electrode materials (CNTs) were examined using a scanning electron microscope (SEM). The vibrational energy modes of CNTs were studied by Raman spectroscopy. X-ray photoelectron spectroscopy (XPS) was used to examine the surface structure of electrode materials. A Brunauer–Emmett–Teller (BET) surface area analyzer was used to examine the specific surface area, pore volume, and pore size of the samples.

Electrochemical Characterization and Fabrication of Symmetric Electrochemical Capacitors. The preparation illustration of the CNT//IL//CNT prototype is shown in Figure 2c. The symmetric CNT//IL//CNT electrochemical capacitors were fabricated without using any conductive agent, binder, and ionic solvent. A two-electrode system (using a Teflon Swagelok-type cell) was used for the investigation of electrochemical performances of as-prepared devices (CNT//IL//CNT). A carbon nanotube film was cut (1 × 1 cm² square, 0.04 mm thickness, mass = 2 mg/electrode, total mass = 4 mg for both electrodes) into pieces and stacked in a Teflon Swagelok-type cell with few drops of ionic liquid electrolyte to form the CNT//IL//CNT devices. An Autolab PGSTAT204 was used to investigate the electrochemical measurements of the as-prepared devices. The electrochemical performances of as-fabricated devices were measured by galvanostatic charge–discharge (GCD), electrochemical impedance spectroscopy (EIS), and cyclic voltammetry (CV) techniques. The GCD and CV data were recorded at various current densities (0.5–2.5 A·g⁻¹) and scan rates (10–100 mV·s⁻¹) in an operational voltage window of 0–4 V. The GCD and CV data were used to calculate the specific capacitance (*C_s*) of as-fabricated devices by using the following equations:⁴³

$$C_s = \frac{i\Delta t}{m\Delta V} \quad (1)$$

$$C_s = \frac{\int IdV}{mv\Delta V} \quad (2)$$

where *m* is the mass of electrodes, *v* is the scan rate, *I* is the current, and ΔV is the voltage window.

The equations used to calculate the power and energy densities are as follows:

$$P = \frac{E \times 3600}{\Delta t} \quad (3)$$

$$E = \frac{C_s \times \Delta V^2 \times 1000}{2 \times 3600} \quad (4)$$

where Δt is the discharge time, *P* is the power density, *E* is the energy density, ΔV is the operational voltage window, and *C_s* is the specific capacitance.

RESULTS AND DISCUSSION

Structural, Morphological, Compositional, and Surface Analysis of Materials.

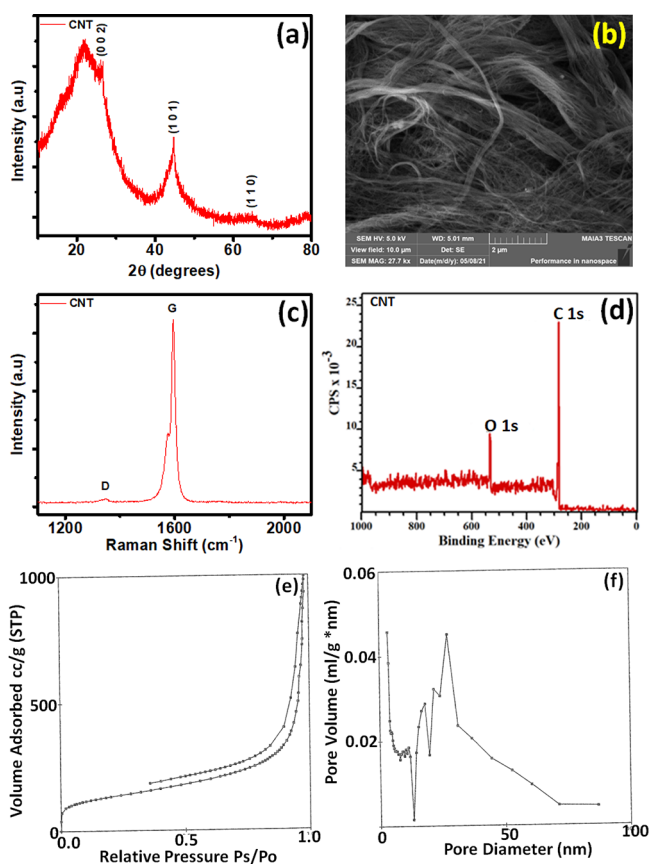


Figure 1. (a) XRD pattern, (b) SEM image, and (c) Raman and (d) XPS spectra of CNTs. (e, f) N₂ adsorption–desorption isotherms and desorption pore volume versus pore diameter of CNTs.

diffraction patterns of CNTs, and a broad and asymmetric peak is observed at $2\theta = \sim 24^\circ$ for amorphous carbon corresponding to the (002) plane. Though the carbon nanotubes have shown an amorphous structure, an enhanced intensity at $2\theta = \sim 44.4^\circ$ for the (101) plane displayed the crystallinity of carbon nanotubes, which replicated the atomic structure of folded sheets of graphene. The peak corresponding to the (110) plane at $2\theta = \sim 63.7^\circ$ further showed the crystallinity of carbon nanotubes. The SEM images of CNTs are displayed in Figure 1b and Figure S1a,b. The SEM images of CNTs show a very dense and long hair-like structure arbitrarily crowding each other at a lower magnification. However, at a higher magnification, the SEM images show a complex network of intersecting fibers (densely packed) that are a few nanometers in diameter and a few microns in length. The fibers are porous, which could further improve ion diffusion and storage in an electrochemical capacitor. The Raman spectra are shown in Figure 1c. The spectra display a small D band peak at ~ 1348 cm⁻¹ and a very sharp G band at ~ 1578 cm⁻¹ due to the sp³ and sp² vibrations of C atoms.⁴⁴ The graphitization of carbon is shown by a narrow and sharp G band (FWHM ~ 15.4 cm⁻¹). The D and G band intensity ratio further identifies the ratio of sp³ and sp² C atoms, which further gives evidence for disorderly domains of CNTs. The bonding states of CNTs were studied by XPS analysis. Figure 1d displays the XPS full survey spectrum of CNTs. The

functional groups of CNTs are further identified by deconvoluted (high-resolution) XPS spectra of O 1s and C 1s, as presented in Figure S1c,d. The O 1s peaks for CNTs are recognized as O–C (532.47 eV) and O=C (533.73 eV), as presented in Figure S1d. As shown in Figure S1d, the C 1s peaks for CNTs are recognized as C–OH (284.77 eV), C=C (284.16 eV), O=C–OH (287.81 eV), and C=O (286.49 eV).⁴⁵ The BET surface area of CNTs was examined under a nitrogen atmosphere, which was confirmed to be $\sim 478 \text{ m}^2/\text{g}$ with a pore volume and average pore size of 1.46 mL/g and 4.87 nm, respectively (Figure 1e,f). The increased surface area results from the porous interconnected morphology of highly dense fiber and long hair-like assemblies that are arbitrarily overflowing with each other. The adsorption/desorption isotherms show slight hysteresis.

Electrochemical Characterization. The capacitive behaviors of CNT//EMIMBF₄//CNT, CNT//EMIMTFSI//CNT, and CNT//BF₄:TFSI//CNT devices were analyzed at different operational voltages, scan rates, and current densities. In addition, to validate the wide applicability of CNT//EMIMBF₄//CNT, CNT//EMIMTFSI//CNT, and CNT//BF₄:TFSI//CNT devices, green (3.3 V) and red (2.1 V) LEDs were lighted up. A mixture of IL electrolytes (EMIMBF₄:EMIMTFSI) was selected as the best electrolyte to achieve high C_s and ED as compared to individual neat EMIMBF₄ and EMIMTFSI. Figure 3a illustrates the relative CV curves for CNT//EMIMBF₄//CNT, CNT//EMIMTFSI//CNT, and CNT//BF₄:TFSI//CNT full devices at 10 mV·s⁻¹. The area under the CV profile of the CNT//BF₄:TFSI//CNT electrode is much higher than those of CNT//EMIMBF₄//CNT and CNT//EMIMTFSI//CNT electrodes, which clearly indicates the enhancement in the electrochemical energy storage. All three devices displayed a wide voltage window as they charged up to 3.5 V for CNT//EMIMBF₄//CNT, 4.0 V for CNT//EMIMTFSI//CNT, and 3.8 V for CNT//BF₄:TFSI//CNT, deprived of any overpotential. Some Faradaic reaction may occur due to impurities in electrolytes or functional groups in CNTs; that is why CV graphs show slight peaks at lower scan rates, which can be clearly seen in Figure 3a. Specifically, the CNT//BF₄:TFSI//CNT device exhibited a higher specific capacitance ($C_s \sim 120 \text{ F}\cdot\text{g}^{-1}$) than CNT//EMIMBF₄//CNT ($C_s \sim 89 \text{ F}\cdot\text{g}^{-1}$) and CNT//EMIMTFSI//CNT ($C_s \sim 73 \text{ F}\cdot\text{g}^{-1}$) devices at 10 mV·s⁻¹. An enhanced C_s of the CNT//BF₄:TFSI//CNT device is due to combined anion structure (BF₄⁻ and TFSI⁻) and properties of both ILs as compared to neat EMIMBF₄ and EMIMTFSI individual electrolytes. However, the higher C_s of the CNT//EMIMBF₄//CNT device than the CNT//EMIMTFSI//CNT device is due to the fast ion transport, smaller anion size, and high conductivity of EMIMBF₄ than the EMIMTFSI electrolyte.

The cationic and anionic structures of ILs are presented in Figure 2a, and the charge storage mechanism is shown in Figure 4a–f. Due to the larger anion size of TFSI⁻ as compared to BF₄⁻, the movement of ions is much slower in CNT//EMIMTFSI//CNT than in CNT//EMIMBF₄//CNT, which further affects the charge storability and capacitance of the device, as shown in Figure 4g. The correlation between the EDL capacitance and anion size of the IL was also explained by Wang et al.⁴⁶ They reported that an increase in anion size constrains the ionic mobility, which further increases the charging time and EDL thickness. Figure 3c shows the CV profile of the CNT//EMIMBF₄//CNT device at various scan rates (10 to 100 mV/s). It is remarkable to note that even at higher scan rates, all three

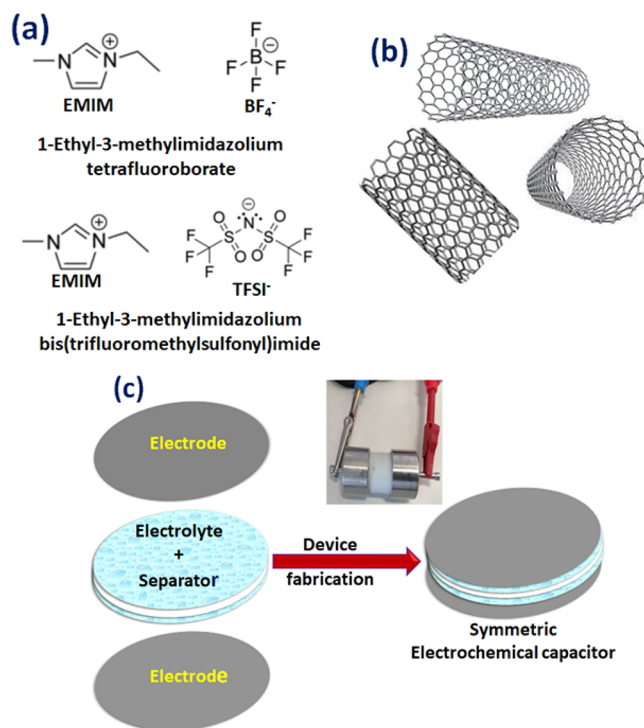


Figure 2. (a) Abbreviations and structures of the anions and cations of ionic liquids. (b) Structure of CNTs. (c) Graphical illustration of the fabrication of symmetric electrochemical capacitors.

devices maintain their charge storability and rectangular shape, which signifies the stability of all three devices at higher scan rates. With an increase in scan rates, the C_s decreases for all three devices as displayed in Table S1 and Figure 3b. The corresponding CV graphs at various scan rates for all three devices are displayed in Figure 3c–e, respectively. The CNT fibers are porous in nature, which further improves the ion diffusion and storage in electrochemical capacitors as discussed before.

The schematic illustration of the development of EDLC layers on CNT electrodes at the charging process and mobility of ions back in solvent at the time of discharging process for all three devices is shown in Figure 4a–f. In the porous CNT electrodes, there is sufficient space for the accumulation of multiple layers of BF₄⁻ anion at the electrode–electrolyte interface as compared to the TFSI⁻ anion, which is due to the low molecular weight, small size (2.6 Å), and high hydrolytic and thermal stability of BF₄⁻, as shown in figure 4a–d. Therefore, the CNT//EMIMBF₄//CNT device has shown improved electrochemical performance compared to the CNT//EMIMTFSI//CNT device. However, in the case of IL mixture (BF₄:TFSI), the combined anion structure and properties play significant part in the improvement of the electrochemical performance of the CNT//BF₄:TFSI//CNT device, as shown in Figure 4e,f). Due to the larger anion size of TFSI⁻ as compared to BF₄⁻, the movement of ions is much slower in CNT//EMIMTFSI//CNT than in CNT//EMIMBF₄//CNT, which further affects the charge storability and capacitance of the device, as shown in Figure 4g. On the other hand, the mixed ionic liquid electrolyte has the same cations but different anions (BF₄⁻ and TFSI⁻), which help to improve the ion diffusion and operating voltage window simultaneously and further improve the capacitance of the device.

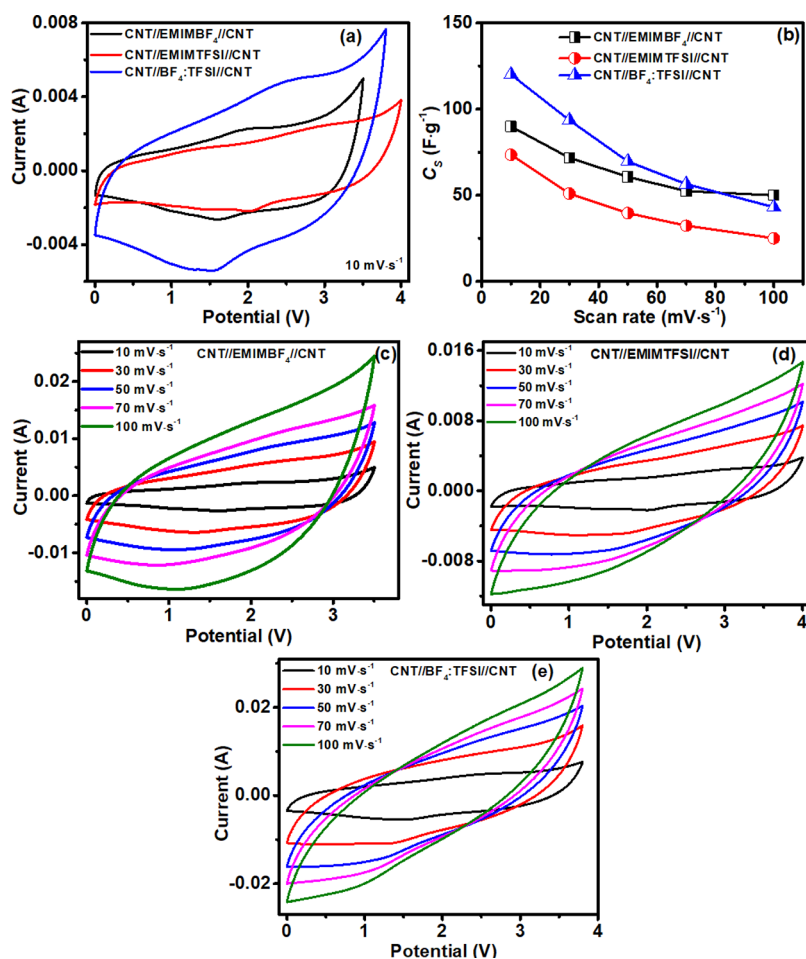


Figure 3. (a) Compared cyclic voltammograms (CVs) of CNT//EMIMBF₄//CNT, CNT//EMIMTFSI//CNT, and CNT//BF₄:TFSI//CNT full devices at 10 mV·s⁻¹. (b) Calculated C_s for CNT//EMIMBF₄//CNT, CNT//EMIMTFSI//CNT, and CNT//BF₄:TFSI//CNT full devices at various scan rates. (c–e) CV graphs of CNT//EMIMBF₄//CNT, CNT//EMIMTFSI//CNT, and CNT//BF₄:TFSI//CNT full devices at various scan rates.

The superior electrochemical properties, mainly for the CNT//BF₄:TFSI//CNT device, were further identified by GCD studies, as displayed in Figure 5a,b. The compared GCD graphs for CNT//EMIMBF₄//CNT, CNT//EMIMTFSI//CNT, and CNT//BF₄:TFSI//CNT devices are displayed in Figure 5a, which are almost triangular in shape because of the charge storage mechanism (EDLC). Correspondingly, the C_s values were found to be 79 F·g⁻¹ at 0.25 A·g⁻¹ for the CNT//BF₄:TFSI//CNT device, whereas the CNT//EMIMBF₄//CNT and CNT//EMIMTFSI//CNT devices showed C_s values of 57 and 41.37 F·g⁻¹ at 0.25 A·g⁻¹. The higher C_s of the CNT//BF₄:TFSI//CNT device is due to the combined anion structure (BF₄ and TFSI) and properties of both ILs as compared to neat EMIMBF₄ and EMIMTFSI individual electrolytes. However, the higher C_s of CNT//EMIMBF₄//CNT than the CNT//EMIMTFSI//CNT device is due to the fast ion transport, smaller anion size, and high conductivity of EMIMBF₄ than the EMIMTFSI electrolyte. The structure of ionic liquids is shown in Figure 2a, and the charge storage mechanism is shown in Figure 4a–f. Due to the larger anion size of TFSI⁻ as compared to BF₄⁻, the movement of ions is significantly slower in CNT//EMIMTFSI//CNT than in CNT//EMIMBF₄//CNT, which further affects the charge storability and capacitance of the device. Anions with smaller sizes have higher electrostatic interactions, which further improves the charge-ordering

structures near electrodes. Table S2 and Figure 5b show that the C_s decreases for all three devices by increasing the current densities. At various current densities, the GCD graphs for CNT//EMIMBF₄//CNT, CNT//EMIMTFSI//CNT, and CNT//BF₄:TFSI//CNT devices are displayed in Figure 5c–e. The lighting of a 3.3 V, 50 mA, and 5 mm green LED and 2.1 V, 20 mA, 10 mm red LED by CNT//EMIMBF₄//CNT, CNT//EMIMTFSI//CNT, and CNT//BF₄:TFSI//CNT full devices after charging at 0.5 A·g⁻¹ is shown in Figure 5f–h.

Electrochemical impedance spectroscopy (EIS) analysis was accomplished at a wide frequency range (100 kHz to 100 MHz) to understand the behavior of electrodes and electrolytes at their interfaces. The Nyquist plot helps to understand the electrode's interfacial resistance. Usually, the lesser the semicircle, the lower the charge transfer resistance and the better the electrical conductivity.^{47–49} The CNT//BF₄:TFSI//CNT device showed a smaller semicircle (insets of Figure 6a) than CNT//EMIMTFSI//CNT and CNT//EMIMBF₄//CNT devices, which indicates the less resistance and higher electrical conductivity of the device. The charge-transfer resistance (R_{CT}) and the solution resistance (R_s) can be accomplished from the semicircle intercept and intercept at the Z_{real} from the high-frequency range. The CNT//BF₄:TFSI//CNT device has a lower equivalent series resistance (~5 Ω) than CNT//EMIMBF₄//CNT (~5.3 Ω) and CNT//EMIMTFSI//CNT

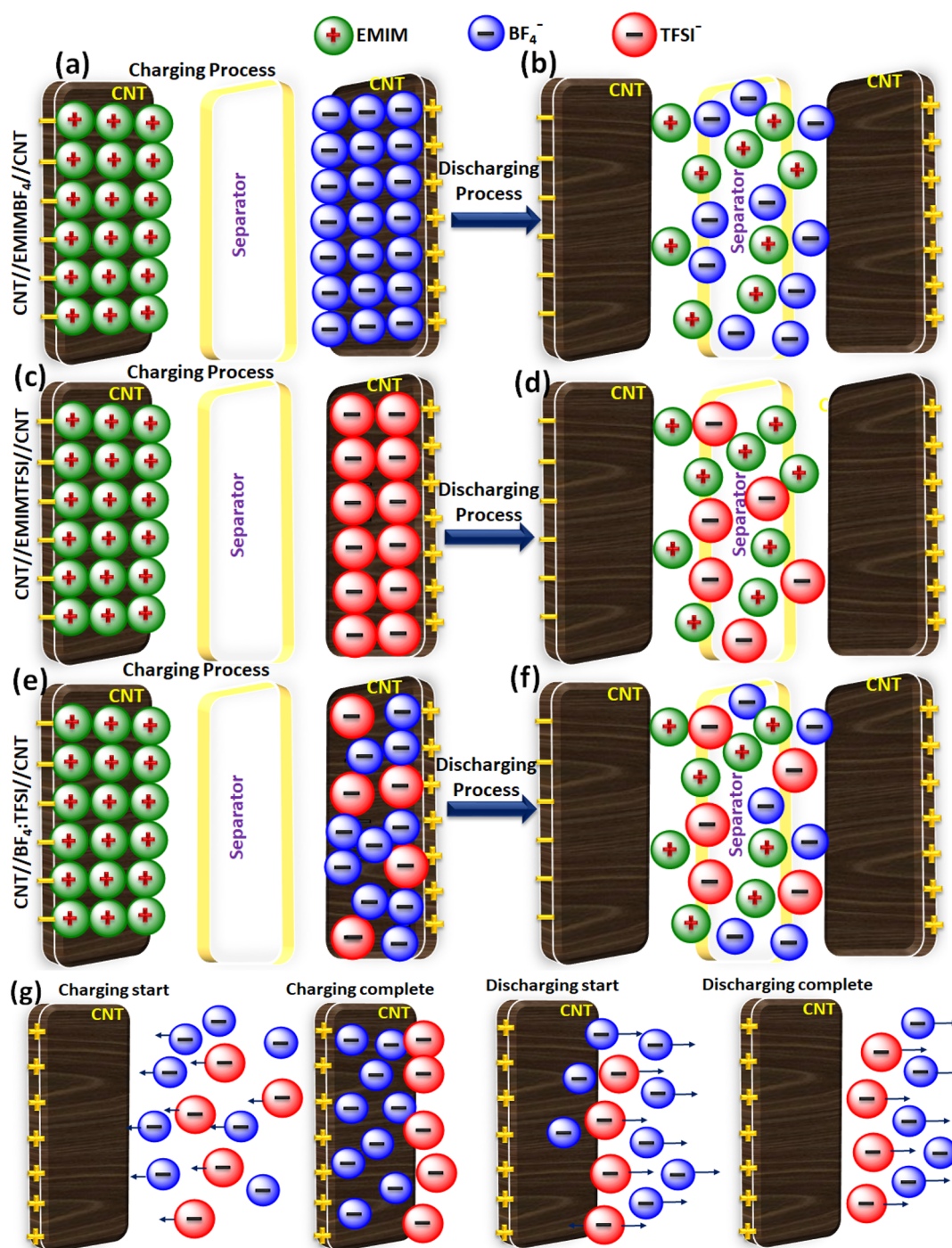


Figure 4. Schematic illustration of development of EDLC layers on CNT electrodes at the time of charging process and mobility of ions back in solvent at the time of discharging process: (a, b) CNT//EMIMBF₄//CNT, (c, d) CNT//EMIMTFSI//CNT, and (e, f) CNT//BF₄:TFSI//CNT full devices. (g) Graphic illustration of comparison of mobility/diffusion of anions (BF₄⁻ and TFSI⁻) on CNT electrodes at the time of charging and discharging process. The mobility of anions depends upon their radius.

devices ($\sim 20 \Omega$), which characterizes the electronic and ionic resistances. Conversely, the CNT//BF₄:TFSI//CNT device displayed a smaller R_{CT} ($\sim 20 \Omega$) as compared to CNT//EMIMBF₄//CNT ($\sim 25 \Omega$) and CNT//EMIMTFSI//CNT ($\sim 70.4 \Omega$) devices. In brief, the low values of R_{CT} and R_s for the CNT//BF₄:TFSI//CNT device indicate its superior electrochemical performance, which was additionally supported by GCD and CV results. Therefore, the EIS results are in well agreement with GDC and CV results, which further verify the

improved electrochemical performance of the CNT//BF₄:TFSI//CNT device.

The power and energy densities of the electrochemical capacitors are very important parameters, and they represent the potential utilization of energy storage devices. The power and energy densities of all three devices were calculated using eqs 3 and 4. Figure 6b displays the compared energy density versus current density graphs for all three symmetrical devices. The CNT//BF₄:TFSI//CNT device showed a higher energy density ($159.5 \text{ Wh}\cdot\text{kg}^{-1}$) than CNT//EMIMBF₄//CNT and CNT//

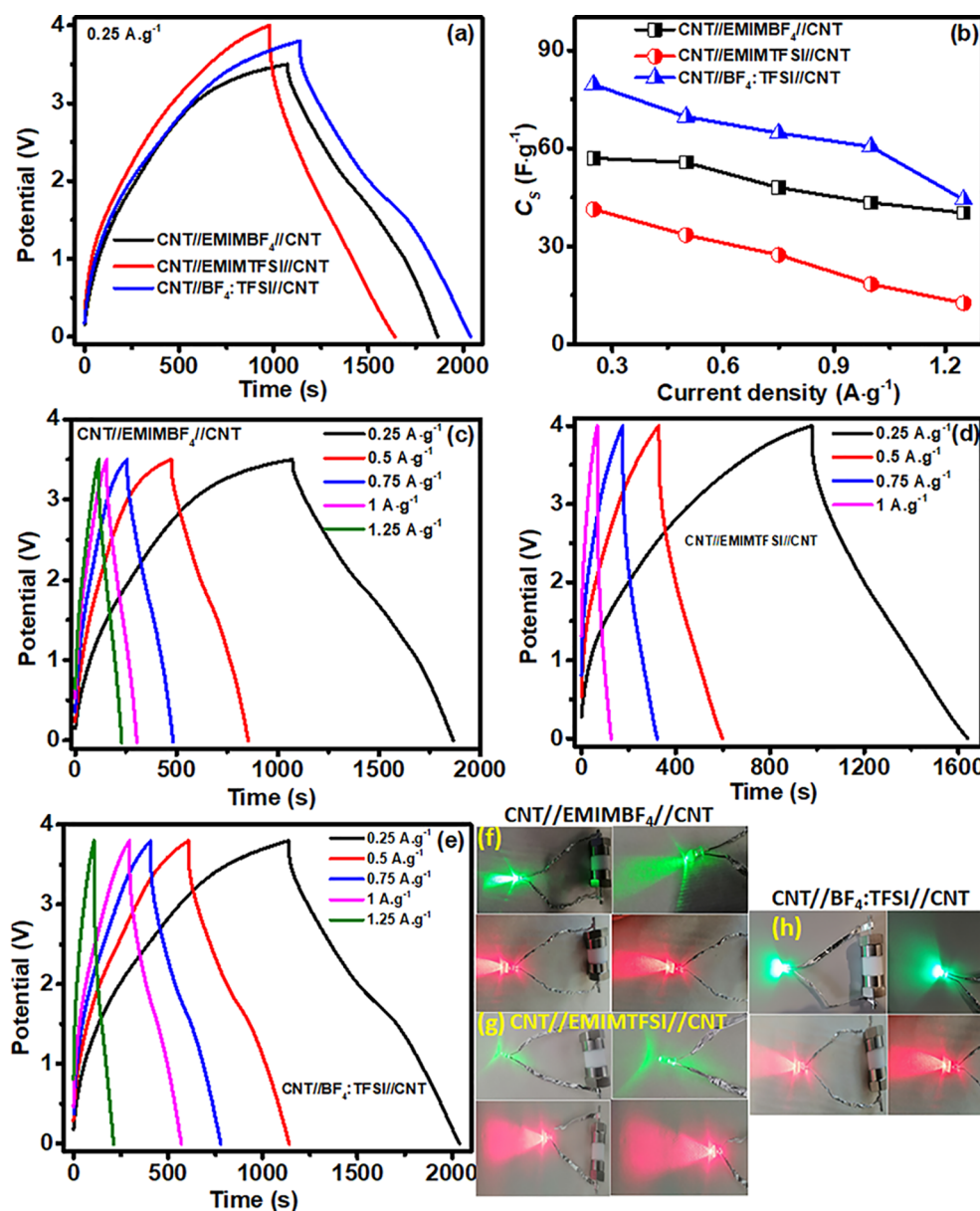


Figure 5. (a) Compared galvanostatic charge–discharge (GCD) graphs of CNT//EMIMBF₄//CNT, CNT//EMIMTFSI//CNT, and CNT//BF₄.TFSI//CNT full devices at 0.5 A.g⁻¹. (b) Calculated C_s for CNT//EMIMBF₄//CNT, CNT//EMIMTFSI//CNT, and CNT//BF₄.TFSI//CNT full devices at various current densities. (c–e) GCD graphs of CNT//EMIMBF₄//CNT, CNT//EMIMTFSI//CNT, and CNT//BF₄.TFSI//CNT full devices at various current densities. (f–h) Lighting of a 3.3 V, 50 mA, and 5 mm green LED and 2.1 V, 20 mA, 10 mm red LED by CNT//EMIMBF₄//CNT, CNT//EMIMTFSI//CNT, and CNT//BF₄.TFSI//CNT full devices after charging at 0.5 A.g⁻¹.

EMIMTFSI//CNT devices (96.97 Wh.kg⁻¹ and 91.21 Wh.kg⁻¹), and the energy density reduces as the current density increases, as displayed in Figure 6b, for all three devices. The obtained energy densities are far superior to the reported energy densities in the literature. The assembled electrochemical capacitors have shown excellent energy densities with different current densities, as shown in Table S3. Figure 6c displays the compared graphs of energy and power densities for all three devices, and the energy densities decrease with an increase in power densities. The CNT//BF₄.TFSI//CNT device showed a high energy density but less power density as compared to CNT//EMIMBF₄//CNT and CNT//EMIMTFSI//CNT devices.

Aside from excellent power and energy densities, a stable life cycle is also important for a suitable energy storage device. The

cycling stability test is a significant key to analyze the performance of an energy storage device. At potential windows of 0–3.5, 0–4, and 0–3.8 V, the cycle stability of the CNT//BF₄.TFSI//CNT, CNT//EMIMBF₄//CNT, and CNT//EMIMTFSI//CNT devices was measured at 0.5 A.g⁻¹ for 500 cycles, as demonstrated in Figure 6d. As illustrated in Figure 6d, the CNT//BF₄.TFSI//CNT device possesses an initial capacitance of 77.7 F.g⁻¹ and retains 34.56 F.g⁻¹ after 500 cycles at 0.5 A.g⁻¹ (ca. 45% of capacitance retention). As illustrated in Figure 6d, the CNT//EMIMBF₄//CNT device possesses an initial capacitance of 55.5 F.g⁻¹ and retains 33.5 F.g⁻¹ after 500 cycles at 0.5 A.g⁻¹ (ca. 60.3% of capacitance retention); the better stability as compared to other devices may be due to its lower operational voltage window. As illustrated in Figure 6d, the CNT//EMIMTFSI//CNT device possesses an

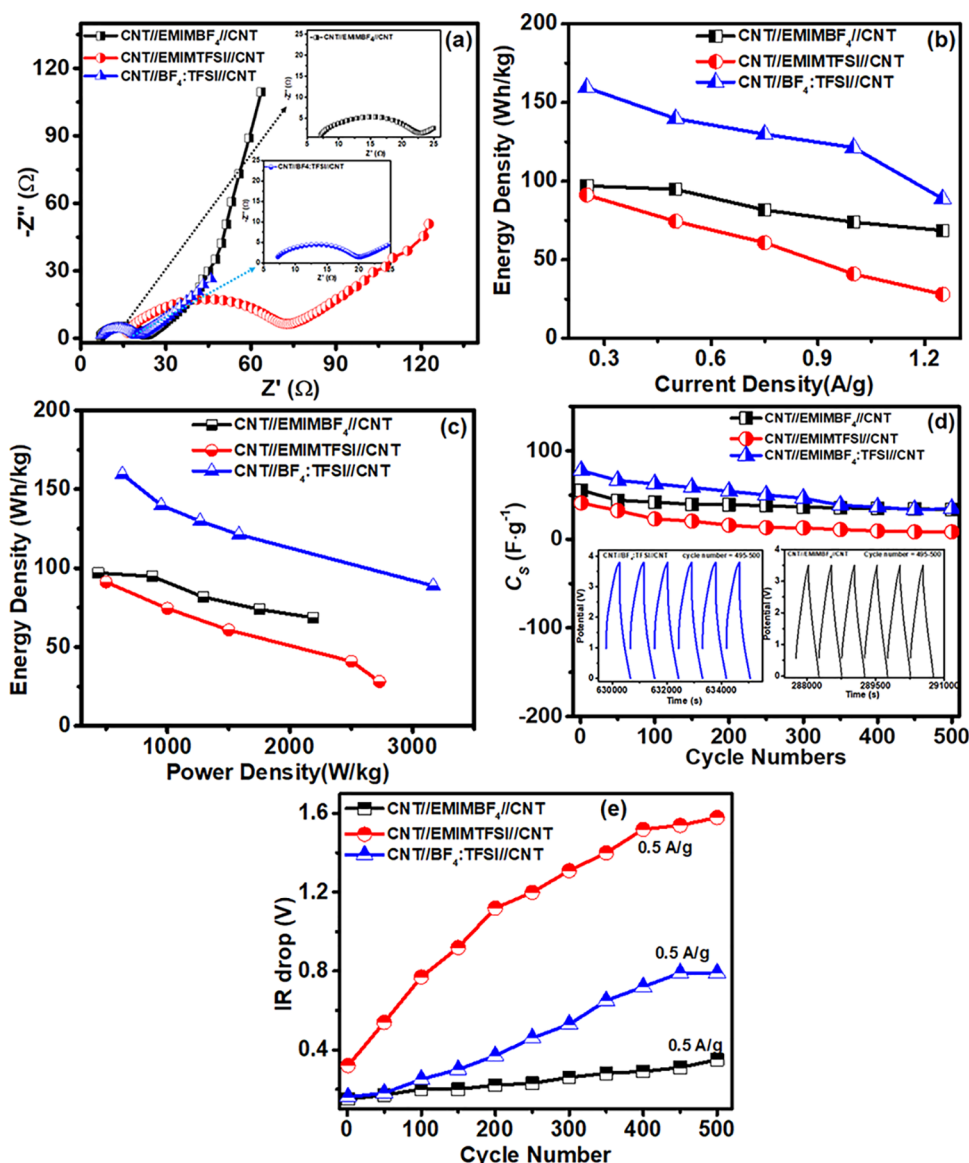


Figure 6. (a) Compared EIS graphs of CNT//EMIMBF₄//CNT, CNT//EMIMTFSI//CNT, and CNT//BF₄:TFSI//CNT full devices. (b) Energy density of CNT//EMIMBF₄//CNT, CNT//EMIMTFSI//CNT, and CNT//BF₄:TFSI//CNT full devices at various current densities. (c) Energy density vs power density of CNT//EMIMBF₄//CNT, CNT//EMIMTFSI//CNT, and CNT//BF₄:TFSI//CNT full devices. (d) C_s versus number of cycles for CNT//EMIMBF₄//CNT, CNT//EMIMTFSI//CNT, and CNT//BF₄:TFSI//CNT at 0.5 A·g⁻¹. (e) IR drop versus cycle number for all three devices.

initial capacitance of 41 F·g⁻¹ and retains 8.5 F·g⁻¹ after 500 cycles at 0.5 A·g⁻¹ (ca. 20.7% of capacitance retention), implying inferior cycle stability, which could be due to a higher operational voltage window. Figure 6e displays the IR drop versus cycle number graph for all three devices. The device resistance increases with an increase in polarization, as displayed by a higher IR drop with the cycling number (Figure 6e). Figure 7a–d shows the compared CV, GCD, EIS, and C_s versus current density graphs for all three devices after 500 cycles. Even after the stability test, all the devices showed the same trend for electrochemical behavior.

CONCLUSIONS

In brief, we studied the charge storage mechanism of binder-free electrochemical capacitors in ionic liquid electrolytes. The device using a mixture of BF₄:TFSI (1:0.5) electrolytes has an operating voltage of 0–3.8 V and excellent device performance

with a C_s retention of ~45% at 0.5 A·g⁻¹ after 500 cycles. In the porous CNT electrodes, there is sufficient space for the accumulation of multiple layers of BF₄⁻ anion at the interface (electrode/electrolyte) as compared to the TFSI⁻ anion, which is due to the low molecular weight, small size (2.6 Å), and high hydrolytic and thermal stability of BF₄⁻. Due to the larger anion size of TFSI⁻ as compared to BF₄⁻, the movement of ions is significantly slower in CNT//EMIMTFSI//CNT than in CNT//EMIMBF₄//CNT, further affecting the charge storability and capacitance of the device. Therefore, the CNT//EMIMBF₄//CNT device has shown an improved electrochemical performance compared to the CNT//EMIMTFSI//CNT device. In the case of IL mixture (BF₄:TFSI), the combined anion structure and properties play a vital role in the improvement of the electrochemical performance of the CNT//BF₄:TFSI//CNT device. The assembled electrochemical

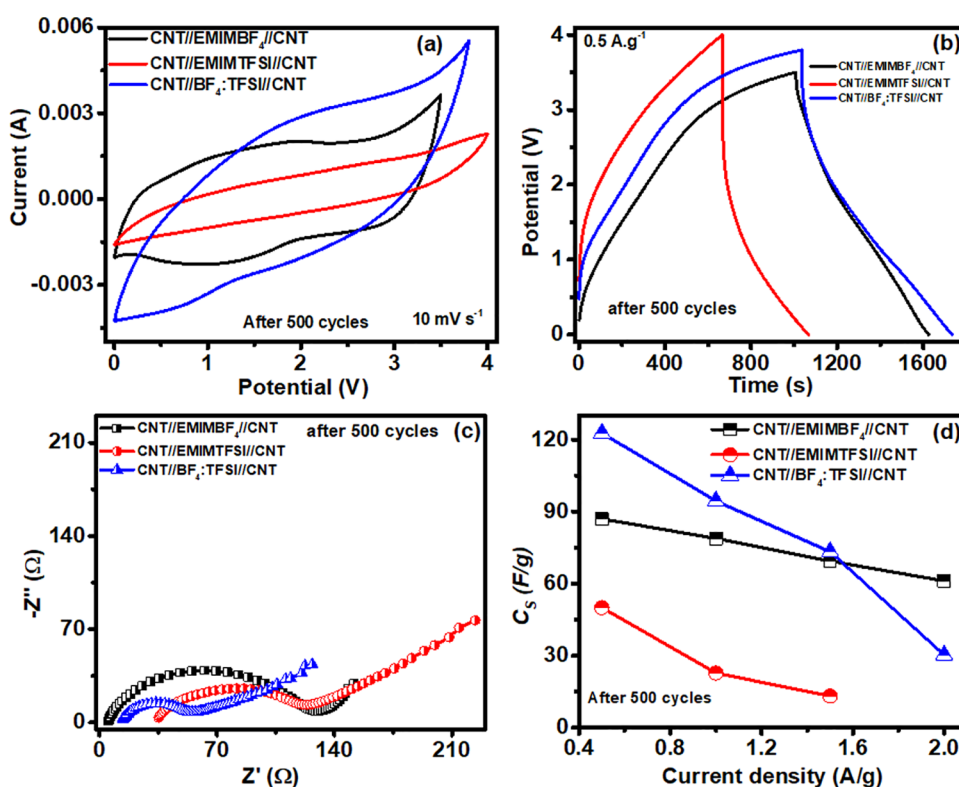


Figure 7. (a) Compared cyclic voltammograms (CVs) of CNT//EMIMBF₄//CNT, CNT//EMIMTFSI//CNT, and CNT//BF₄:TFSI//CNT full devices at 10 mV·s⁻¹ after 500 cycles. (b) Compared galvanostatic charge–discharge (GCD) graphs of CNT//EMIMBF₄//CNT, CNT//EMIMTFSI//CNT, and CNT//BF₄:TFSI//CNT full devices at 0.5 A·g⁻¹ after 500 cycles. (c) Compared EIS graphs of CNT//EMIMBF₄//CNT, CNT//EMIMTFSI//CNT, and CNT//BF₄:TFSI//CNT full devices after 500 cycles. (d) Calculated C_s for CNT//EMIMBF₄//CNT, CNT//EMIMTFSI//CNT, and CNT//BF₄:TFSI//CNT full devices at various current densities after 500 cycles.

capacitor managed to light up green (3.3 V) and red (2.1 V) LEDs for more than 5 min.

■ ASSOCIATED CONTENT

Supporting Information

The Supporting Information is available free of charge at <https://pubs.acs.org/doi/10.1021/acs.iecr.2c03667>.

SEM images of the electrodes, high-resolution XPS spectra, cross-sectional SEM images of CNTs, CV and GCD measurements of full devices, and table of specific capacitance and results of stability tests (CV and GCD measurements) (PDF)

■ AUTHOR INFORMATION

Corresponding Authors

Bhupender Pal – Department of Inorganic Chemistry, University of Chemistry and Technology Prague, 166 28 Prague 6, Czech Republic; Email: palh@vscht.cz

Zdeněk Sofer – Department of Inorganic Chemistry, University of Chemistry and Technology Prague, 166 28 Prague 6, Czech Republic; orcid.org/0000-0002-1391-4448; Email: zdenek.sofer@vscht.cz

Authors

Abhilash Karuthedath Parameswaran – Department of Inorganic Chemistry, University of Chemistry and Technology Prague, 166 28 Prague 6, Czech Republic

Bing Wu – Department of Inorganic Chemistry, University of Chemistry and Technology Prague, 166 28 Prague 6, Czech Republic; orcid.org/0000-0002-9637-6787

Lukáš Děkanovský – Department of Inorganic Chemistry, University of Chemistry and Technology Prague, 166 28 Prague 6, Czech Republic

Vlastimil Mazánek – Department of Inorganic Chemistry, University of Chemistry and Technology Prague, 166 28 Prague 6, Czech Republic

Kalyan Jyoti Sarkar – Department of Inorganic Chemistry, University of Chemistry and Technology Prague, 166 28 Prague 6, Czech Republic

Rajan Jose – Center for Advanced Intelligent Materials, Faculty of Industrial Sciences & Technology, Universiti Malaysia Pahang, Kuantan 26300, Malaysia; orcid.org/0000-0003-4540-321X

Complete contact information is available at <https://pubs.acs.org/doi/10.1021/acs.iecr.2c03667>

Notes

The authors declare no competing financial interest.

■ ACKNOWLEDGMENTS

B.P. acknowledges the European Structural and Investment Funds, CHEMFELLS VI (No. CZ.02.2.69/0.0/0.0/20_079/0017899). Z.S. was supported by Czech Science Foundation (GACR No. 20-16124J). R.J. acknowledges the Research & Innovation Department of Universiti Malaysia Pahang for RDU 203301.

REFERENCES

- (1) Zhai, Y.; Dou, Y.; Zhao, D.; Fulvio, P. F.; Mayes, R. T.; Dai, S. Carbon Materials for Chemical Capacitive Energy Storage. *Adv. Mater.* **2011**, *23*, 4828–4850.
- (2) Walcarius, A. Mesoporous Materials and Electrochemistry. *Chem. Soc. Rev.* **2013**, *42*, 4098–4140.
- (3) MacFarlane, D. R.; Tachikawa, N.; Forsyth, M.; Pringle, J. M.; Howlett, P. C.; Elliott, G. D.; Davis, J. H.; Watanabe, M.; Simon, P.; Angell, C. A. Energy Applications of Ionic Liquids. *Energy Environ. Sci.* **2014**, *7*, 232–250.
- (4) Béguin, F.; Presser, V.; Balducci, A.; Frackowiak, E. Carbons and Electrolytes for Advanced Supercapacitors. *Adv. Mater.* **2014**, *26*, 2219–2251.
- (5) Stoller, M. D.; Park, S.; Zhu, Y.; An, J.; Ruoff, R. S. Graphene-based ultracapacitors. *Nano Lett.* **2008**, *8*, 3498–3502.
- (6) Barbieri, O.; Hahn, M.; Herzog, A.; Kötz, R. Capacitance Limits of High Surface Area Activated Carbons for Double Layer Capacitors. *Carbon* **2005**, *43*, 1303–1310.
- (7) Kötz, R.; Carlen, M. Principles and Applications of Electrochemical Capacitors. *Electrochim. Acta* **2000**, *45*, 2483–2498.
- (8) Xing, W.; Qiao, S. Z.; Ding, R. G.; Li, F.; Lu, G. Q.; Yan, Z. F.; Cheng, H. M. Superior Electric Double Layer Capacitors using Ordered Mesoporous Carbons. *Carbon* **2006**, *44*, 216–224.
- (9) Jeong, H. M.; Lee, J. W.; Shin, W. H.; Choi, Y. J.; Shin, H. J.; Kang, J. K.; Choi, J. W. Nitrogen-Doped Graphene for High-Performance Ultracapacitors and the Importance of Nitrogen-Doped Sites at Basal Planes. *Nano Lett.* **2011**, *11*, 2472–2477.
- (10) Wu, H.; Wang, X.; Jiang, L.; Wu, C.; Zhao, Q.; Liu, X.; Hu, B.; Yi, L. The Effects of Electrolyte on the Supercapacitive Performance of Activated Calcium Carbide-Derived Carbon. *J. Power Sources* **2013**, *226*, 202–209.
- (11) Wang, Y.; Zheng, C.; Qi, L.; Yoshio, M.; Yoshizuka, K.; Wang, H. Utilization of (oxalato) Borate-Based Organic Electrolytes in Activated Carbon/Graphite Capacitors. *J. Power Sources* **2011**, *196*, 10507–10510.
- (12) Lewandowski, A.; Świdorska, A. Electrochemical Capacitors with Polymer Electrolytes Based on Ionic Liquids. *Solid State Ionics* **2003**, *161*, 243–249.
- (13) Galiński, M.; Lewandowski, A.; Stępnik, I. Ionic Liquids as Electrolytes. *Electrochim. Acta* **2006**, *51*, 5567–5580.
- (14) Pal, B.; Yang, S.; Ramesh, S.; Thangadurai, V.; Jose, R. Electrolyte Selection for Supercapacitive Devices: A Critical Review. *Nanoscale Adv.* **2019**, *1*, 3807–3835.
- (15) De Vos, N.; Maton, C.; Stevens, C. V. Electrochemical Stability of Ionic Liquids: General Influences and Degradation Mechanisms. *ChemElectroChem* **2014**, *1*, 1258–1270.
- (16) Arbizzani, C.; Biso, M.; Cericola, D.; Lazzari, M.; Soavi, F.; Mastragostino, M. Safe, High-Energy Supercapacitors Based on Solvent-Free Ionic Liquid Electrolytes. *J. Power Sources* **2008**, *185*, 1575–1579.
- (17) Fitchett, B. D.; Knepp, T. N.; Conboy, J. C. 1-Alkyl-3-Methylimidazolium bis (Perfluoroalkylsulfonyle) Imide Water-Immiscible Ionic Liquids: the Effect of Water on Electrochemical and Physical Properties. *J. Electrochem. Soc.* **2004**, *151*, E219.
- (18) Appetecchi, G. B.; Montanino, M.; Zane, D.; Carewska, M.; Alessandrini, F.; Passerini, S. Effect of the Alkyl Group on the Synthesis and the Electrochemical Properties of N-alkyl-N-methyl-pyrrolidinium bis (trifluoromethanesulfonyl) Imide Ionic Liquids. *Electrochim. Acta* **2009**, *54*, 1325–1332.
- (19) Montanino, M.; Carewska, M.; Alessandrini, F.; Passerini, S.; Appetecchi, G. B. The Role of the Cation Slipathic Side Chain Length in Piperidinium bis (Trifluoromethanesulfonyl) Imide Ionic Liquids. *Electrochim. Acta* **2011**, *57*, 153–159.
- (20) Lockett, V.; Sedev, R.; Ralston, J.; Horne, M.; Rodopoulos, T. Differential Capacitance of the Electrical Double Layer in Imidazolium-Based Ionic Liquids: Influence of Potential, Cation Size, and Temperature. *J. Phys. Chem. C* **2008**, *112*, 7486–7495.
- (21) Lewandowski, A.; Galiński, M. Carbon-Ionic Liquid Double-Layer Capacitors. *J. Phys. Chem. Solids* **2004**, *65*, 281–286.
- (22) Yoshimura, M.; Honda, K.; Kondo, T.; Uchikado, R.; Einaga, Y.; Rao, T. N.; Tryk, D. A.; Fujishima, A. Factors Controlling the Electrochemical Potential Window for Diamond Electrodes in Non-Aqueous Electrolytes. *Diamond Relat. Mater.* **2002**, *11*, 67–74.
- (23) Yuyama, K.; Masuda, G.; Yoshida, H.; Sato, T. Ionic Liquids Containing the Tetrafluoroborate Anion have the Best Performance and Stability for Electric Double Layer Capacitor Applications. *J. Power Sources* **2006**, *162*, 1401–1408.
- (24) Lang, C. M.; Kim, K.; Guerra, L.; Kohl, P. A. Cation Electrochemical Stability in Chloroaluminate Ionic Liquids. *J. Phys. Chem. B* **2005**, *109*, 19454–19462.
- (25) Lai, F.; Feng, J.; Yan, R.; Wang, G. C.; Antonietti, M.; Oschatz, M. Breaking the Limits of Ionic Liquid-Based Supercapacitors: Mesoporous Carbon Electrodes Functionalized with Manganese Oxide Nanosplotches for Dense, Stable, and Wide-Temperature Energy Storage. *Adv. Funct. Mater.* **2018**, *28*, No. 1801298.
- (26) Mansuer, M.; Miao, L.; Zhu, D.; Duan, H.; Lv, Y.; Li, L.; Liu, M.; Gan, L. Facile Construction of Highly Redox Active Carbons with Regular Micropores and Rod-Like Morphology Towards High-Energy Supercapacitors. *Mater. Chem. Front.* **2021**, *5*, 3061–3072.
- (27) Xia, X.; Zhan, J.; Zhong, Y.; Wang, X.; Tu, J.; Fan, H. J. Crystalline, Metallic TiC Nanowires for Highly Robust and Wide-Temperature Electrochemical Energy Storage. *Small* **2017**, *13*, No. 1602742.
- (28) Bi, S.; Banda, H.; Chen, M.; Niu, L.; Chen, M.; Wu, T.; Wang, J.; Wang, R.; Feng, J.; Chen, T.; Dincă, M.; Kornyshev, A. A.; Feng, G. Molecular Understanding of Charge Storage and Charging Dynamics in Supercapacitors with MOF Electrodes and Ionic Liquid Electrolytes. *Nat. Mater.* **2020**, *19*, 552–558.
- (29) Song, Z.; Miao, L.; Li, L.; Zhu, D.; Lv, Y.; Xiong, W.; Duan, H.; Wang, Z.; Gan, L.; Liu, M. A Universal Strategy to Obtain Highly Redox-Active Porous Carbons for Efficient Energy Storage. *J. Mater. Chem. A* **2020**, *8*, 3717–3725.
- (30) Feng, L.; Wang, K.; Zhang, X.; Sun, X.; Li, C.; Ge, X.; Ma, Y. Flexible Solid-State Supercapacitors with Enhanced Performance from Hierarchically Graphene Nanocomposite Electrodes and Ionic Liquid Incorporated Gel Polymer Electrolyte. *Adv. Funct. Mater.* **2018**, *28*, No. 1704463.
- (31) Liu, X.; Guo, J.; Chen, J.; Zhang, J.; Zhang, J. Synergistic Effect of Ionic Liquid Intercalation and Multiwalled Carbon Nanotube Spacers with Improved Supercapacitor Performance. *J. Power Sources* **2017**, *363*, 54–60.
- (32) Xue, D.; Zhu, D.; Duan, H.; Wang, Z.; Lv, Y.; Xiong, W.; Li, L.; Liu, M.; Gan, L. Deep-Eutectic-Solvent Synthesis of N/O Self-Doped Hollow Carbon Nanorods for Efficient Energy Storage. *Chem. Commun.* **2019**, *55*, 11219–11222.
- (33) Miao, L.; Duan, H.; Zhu, D.; Lv, Y.; Gan, L.; Li, L.; Liu, M. Boron “Gluing” Nitrogen Heteroatoms in a Prepolymerized Ionic Liquid-Based Carbon Scaffold for Durable Supercapacitive Activity. *J. Mater. Chem. A* **2021**, *9*, 2714–2724.
- (34) Li, C.; Zhang, X.; Wang, K.; Sun, X.; Liu, G.; Li, J.; Tian, H.; Li, J.; Ma, Y. Scalable Self-Propagating High-Temperature Synthesis of Graphene for Supercapacitors with Superior Power Density and Cyclic Stability. *Adv. Mater.* **2017**, *29*, No. 1604690.
- (35) She, Z.; Ghosh, D.; Pope, M. A. Decorating Graphene Oxide with Ionic Liquid Nanodroplets: an Approach Leading to Energy-Dense, High-Voltage Supercapacitors. *ACS Nano* **2017**, *11*, 10077–10087.
- (36) Pan, Z.; Yang, J.; Zhang, Q.; Liu, M.; Hu, Y.; Kou, Z.; Liu, N.; Yang, X.; Ding, X.; Chen, H.; Li, J.; Zhang, K.; Qiu, Y.; Li, Q.; Wang, J.; Wang, Y. Solid-State Fiber Supercapacitors with Ultrahigh Volumetric Energy Density and Outstanding Flexibility. *Adv. Energy Mater.* **2019**, *9*, No. 1802753.
- (37) Nguyen, Q. D.; Patra, J.; Hsieh, C. T.; Li, J.; Dong, Q. F.; Chang, J. K. Supercapacitive Properties of Micropore-and Mesopore-Rich Activated Carbon in Ionic-Liquid Electrolytes with Various Constituent Ions. *ChemSusChem* **2019**, *12*, 449–456.
- (38) Khan, I. A.; Shah, F. U. Fluorine-Free Ionic Liquid-Based Electrolyte for Supercapacitors Operating at Elevated Temperatures. *Chem. Eng.* **2020**, *8*, 10212–10221.

(39) Wang, X.; Zhou, H.; Sheridan, E.; Walmsley, J. C.; Ren, D.; Chen, D. Geometrically Confined Favourable Ion Packing for High Gravimetric Capacitance in Carbon–Ionic Liquid Supercapacitors. *Energy Environ. Sci.* **2016**, *9*, 232–239.

(40) Liu, H.; Zhu, G. The Electrochemical Capacitance of Nanoporous Carbons in Aqueous and Ionic Liquids. *J. Power Sources* **2007**, *171*, 1054–1061.

(41) Largeot, C.; Portet, C.; Chmiola, J.; Taberna, P.-L.; Gogotsi, Y.; Simon, P. Relation Between the Ion Size and Pore Size for an Electric Double-Layer Capacitor. *J. Am. Chem. Soc.* **2008**, *130*, 2730–2731.

(42) Gryglewicz, G.; Machnikowski, J.; Lorenc-Grabowska, E.; Lota, G.; Frackowiak, E. Effect of Pore Size Distribution of Coal-Based Activated Carbons on Double Layer Capacitance. *Electrochim. Acta* **2005**, *50*, 1197–1206.

(43) Pal, B.; Matsoso, J. B.; Parameswaran, A. K.; Roy, P. K.; Lukas, D.; Luxa, J.; Marvan, P.; Azadmanjiri, J.; Hrdlicka, Z.; Jose, R.; Sofer, Z. Flexible, Ultralight, and High-Energy Density Electrochemical Capacitors Using Sustainable Materials. *Electrochim. Acta* **2022**, No. 140239.

(44) Qi, H.; Schulz, B.; Vad, T.; Liu, J.; Mäder, E.; Seide, G.; Gries, T. Novel Carbon Nanotube/Cellulose Composite Fibers as Multifunctional Materials. *ACS Appl. Mater. Interfaces* **2015**, *7*, 22404–22412.

(45) Avendano, C.; Brun, N.; Fontaine, O.; In, M.; Mehdi, A.; Stocco, A.; Vioux, A. Multiwalled Carbon Nanotube/Cellulose Composite: from Aqueous Dispersions to Pickering Emulsions. *Langmuir* **2016**, *32*, 3907–3916.

(46) Wang, S.; Li, S.; Cao, Z.; Yan, T. Molecular Dynamic Simulations of Ionic Liquids at Graphite Surface. *Phys. Chem. C* **2010**, *114*, 990–995.

(47) Chung, D. Y.; Lee, K. J.; Yu, S. H.; Kim, M.; Lee, S. Y.; Kim, O. H.; Park, H. J.; Sung, Y. E. Alveoli-Inspired Facile Transport Structure of N-Doped Porous Carbon for Electrochemical Energy Applications. *Adv. Energy Mater.* **2015**, *5*, No. 1401309.

(48) Qin, Y.; Miao, L.; Mansuer, M.; Hu, C.; Lv, Y.; Gan, L.; Liu, M. Spatial Confinement Strategy for Micelle-Size-Mediated Modulation of Mesopores in Hierarchical Porous Carbon Nanosheets with an Efficient Capacitive Response. *ACS Appl. Mater. Interfaces* **2022**, *14*, 33328–33339.

(49) Song, Z.; Miao, L.; Ruhlmann, L.; Lv, Y.; Zhu, D.; Li, L.; Gan, L.; Liu, M. Lewis Pair Interaction Self-Assembly of Carbon Superstructures Harvesting High-Energy and Ultralong-Life Zinc-Ion Storage. *Adv. Funct. Mater.* **2022**, *32*, No. 2208049.

Recommended by ACS

Salt-Concentrated Siloxane-Based Electrolytes for Lithium Metal Batteries: Physical Properties, Electrochemical Properties, and Cell Performance

Asuman Celik-Kucuk and Takeshi Abe

APRIL 21, 2023

ACS APPLIED ENERGY MATERIALS

READ 

Strategy for Stable Interface in Lithium Metal Batteries: Free Solvent Derived vs Anion Derived

Gyuleen Park, Jang Wook Choi, *et al.*

NOVEMBER 03, 2022

ACS ENERGY LETTERS

READ 

Molecular Insights into the Effect of Asymmetric Anions on Lithium Coordination and Transport Properties in Salt-Doped Poly(ionic liquid) Electrolytes

Jiajia Li, Zhen Yang, *et al.*

JULY 22, 2022

MACROMOLECULES

READ 

Exploration of Charge Storage Behavior of Binder-Free EDL Capacitors in Aqueous Electrolytes

Bhupender Pal, Zdeněk Sofer, *et al.*

JANUARY 05, 2023

ACS OMEGA

READ 

Get More Suggestions >